Two functionally distinct HEATR5 protein complexes are defined by fast-evolving co-factors in yeast

Lucas J. Marmorale[1,2]*, Huan Jin[1]*, Thomas G. Reidy[1,3], Brandon Palomino-Alonso[1], Christopher Zysnarski[1,] , Fatima Jordan-Javed[1,4], Sagar Lahiri[1,5], Mara C Duncan[1,6]

1. **Department of Cell and Developmental Biology, University of Michigan, Ann Arbor MI**
2. **Present address: Department of Molecular and Cellular Biology, University of Arizona, Tucson, AZ (ORCID 0000-0001-8926-4368)**
3. **Present address: Department of Biological Sciences, University of Pittsburgh, Pittsburgh, PA (ORCID 0009-0008-4340-612X)**
4. **ORCID 0000-0002-5939-8039**
5. **ORCID 0000-0002-9563-6188.**
6. **Corresponding author:**

   Mara C Duncan (ORCID 0000-0002-2383-0109)

   109 Zina Pitcher Place,

   Ann Arbor,

   Michigan 48109

***Equal Contribution**

Running title: Lft1 defines a second HEATR5 complex

Abstract:

The highly conserved HEATR5 proteins are best known for their roles in membrane traffic mediated by the adaptor protein complex-1 (AP1). HEATR5 proteins rely on fast-evolving co-factors to bind to AP1. However, how HEATR5 proteins interact with these co-factors is unknown. Here, we report that the budding yeast HEATR5 protein, Laa1, functions in two biochemically distinct complexes. These complexes are defined by a pair of mutually exclusive Laa1-binding proteins, Laa2 and the previously uncharacterized Lft1/Yml037c. Despite limited sequence similarity, biochemical analysis and structure predictions indicate that Lft1 and Laa2 bind Laa1 via structurally similar mechanisms. Both Laa1 complexes function in intra-Golgi recycling. However, only the Laa2-Laa1 complex binds to AP1 and contributes to its localization. Finally, structure predictions indicate that human HEATR5 proteins bind to a pair of fast-evolving interacting partners via a mechanism similar to that observed in yeast. These results reveal mechanistic insight into how HEATR5 proteins bind their co-factors and indicate that Laa1 performs functions besides recruiting AP1.

Introduction:

Membrane trafficking impacts nearly every aspect of cell physiology by regulating the proteomes of numerous organelles, including the Golgi, plasma membrane, endosomes, and lysosomes. Many trafficking pathways rely on soluble proteins that assemble into a proteinaceous coat on the cytosolic surface of membranes. The coat selects protein cargo, deforms the membrane, and ultimately pinches the membrane off into a spherical, tubular, or more complicated transport carrier. Consistent with this fundamental role of coat proteins in maintaining organelle function, mutations in coat proteins can cause devastating human diseases (Duncan, 2022; Sanger et al., 2019; Shin et al., 2021).

44 Despite decades of research, many coat components remain poorly characterized, including the highly
45 conserved HEATR5 protein family. This family includes Laa1 in budding yeast, Sip1 in fission yeast,
46 SOAP-1 in worms, HEATR5B in flies (also known as CG2747), HEATR5B and HEATR5A in mammals
47 (also known as p200a and p200b), and Sweetie in plants (Fernandez and Payne, 2006; Gillard et al., 2015;
48 Le Bras et al., 2012; Yu et al., 2012). HEATR5 is essential in flies, worms, and mice, and mutations in
49 HEATR5B cause severe disease in humans (Ghosh et al., 2021; Gillard et al., 2015; Le Bras et al., 2012).
50 However, our knowledge about the mechanisms and functions of HEATR5 proteins is limited.

51 HEATR5 proteins localize to the trans-Golgi network and endosomes and are mainly thought to promote
52 AP1 localization to membranes. HEATR5 proteins bind to AP1 indirectly via one or more fast-evolving
53 co-factors. In budding yeast, Laa1 forms a complex with the co-factor Laa2, which mediates the
54 interaction with AP1 (Kuznetsov et al., 2023; Zysnarski et al., 2019). In humans, HEATR5b
55 simultaneously binds two co-factors, aftiphilin, and γ-synergin, which interact directly with AP1 and are
56 thought to mediate its interaction with HEATR5b (Hirst et al., 2005; Kuznetsov et al., 2023). However, it
57 remains unknown how HEATR5 proteins bind these critical co-factors and whether HEATR5 proteins
58 perform functions in addition to promoting AP1 membrane localization.

59 In the present study, we sought to clarify the molecular mechanisms of the yeast HEATR5 protein Laa1
60 by identifying new co-factors. We identified a previously uncharacterized protein, Yml037c, as a novel
61 Laa1 co-factor. We refer to Yml037c as Lft1 for ***L**aa1 **F**unction **T**wo 1.* We defined how Lft1 and Laa2
62 bind Laa1 and revealed that they form mutually exclusive complexes with Laa1. In addition, we showed
63 that the Lft1-Laa1 complex does not contribute to AP1 localization. These findings suggest that Laa1 has
64 functions besides promoting AP1 membrane localization. Finally, we determined that human HEATR5
65 proteins likely use an interface similar to that found in yeast to bind to a pair of mutually exclusive co-

66 factors. Together, these findings indicate that HEATR5 proteins likely play multiple roles in membrane
67 traffic.

68 **Identification of Lft1**

69 Laa1 is a large protein with the potential to make many physical interactions, however it is only known to
70 interact directly with Laa2. We hypothesized that if the yeast genome encoded additional Laa1 co-factors,
71 the deletion of such co-factors would have similar phenotypes to the deletion of *LAA1*. Therefore, we
72 examined the HOP-profile dataset, which contains information about the growth effect of ~1800 different
73 chemical treatments on gene deletion strains in the yeast deletion collection (Hoepfner et al., 2014). We
74 looked for gene deletions whose sensitivity and resistance profiles correlate with those of *laa1Δ*. Among
75 the top twenty-five correlated genes, we found several genes previously known to disrupt AP1 functions
76 and a single uncharacterized gene *YML037c*, which, based on the results described below, we refer to as
77 Lft1 (*Laa1 Function Two 1*).

78 Lft1 colocalizes with clathrin at the *trans*-Golgi Network (TGN) (Huh et al., 2003). We first determined
79 its localization by tagging the endogenous locus with mCherry and performing co-localization analysis
80 with several markers of the TGN. The TGN in yeast is a dynamically maturing compartment, and its
81 maturation state is associated with waves of traffic, each mediated by different coats (Casler et al., 2019;
82 Daboussi et al., 2012; Highland and Fromme, 2021; Tojima et al., 2019). The clathrin adaptor Gga2
83 mediates the earliest waves, whereas the clathrin adaptor Ent5 and AP1 mediate subsequent waves (Casler
84 et al., 2019). We found that Lft1 colocalized better with Ent5 and AP1 than with Gga2 (Fig. 1), suggesting
85 that it arrives at later stages of TGN maturation.

86 We then asked about the co-localization with Laa1, whose timing with relationship to the other adaptors
87 has not been investigated. Lft1 colocalized more strongly with Laa1 than it did with Ent5 or AP1. When

88 analyzed as Lft1 structures that were positive for Laa1, nearly 80% of Lft1 structures were also positive
89 for Laa1. This result suggests that Lft1 is localized to later-stage TGN, and these are enriched in Laa1
90 compared to other TGN coat components tested. The actual level of co-localization between Lft1 and
91 Laa1 may be slightly higher than reported here since the images were collected on live cells. Therefore,
92 movement or other dynamic behavior could occur during the ~700ms between images. When analyzed as
93 Laa1 structures that were also positive for Lft1, 60% of Laa1 puncta were positive for Lft1. The lower
94 percentage of Laa1 structures that contain Lft1 suggests that a fraction of Laa1 structures are likely devoid
95 of Lft1.

96 To determine whether Lft1 interacted with Laa1, we tagged Lft1 with the HA epitope at its endogenous
97 locus and performed co-immunoprecipitation with Laa1 tagged with the FLAG epitope at its endogenous
98 locus. We found that Lft1 interacted with Laa1 (Fig. 2A). We next asked whether Lft1 localization
99 depends on Laa1. We tagged Lft1 with GFP at its endogenous locus and compared its localization in wild-
100 type and cells lacking Laa1. In wild-type cells, Lft1-GFP localizes to multiple puncta. In cells lacking
101 Laa1, this localization is abolished (Fig. 2B, C). Because Lft1-GFP puncta were completely undetectable,
102 we sought to determine if Laa1 altered Lft1 abundance. To do this, we monitored Lft1-HA abundance in
103 cells lacking Laa1 by immunoblot analysis. Lft1-HA abundance was dramatically lower in cells lacking
104 Laa1 (Fig. 2D, E). This lower abundance suggests that Lft1 is destabilized in the absence of Laa1 and
105 indicates that Lft1 forms an obligate complex with Laa1.

106 **Lft1 and Laa2 are mutually exclusive for binding to Laa1**

107 Because Laa1 is known to form a complex with Laa2 and Laa2 is important for Laa1 localization
108 (Zysnarski et al., 2019), we asked whether loss of Laa2 disrupts Lft1 localization. In contrast to the effect
109 of Laa1, we found that the loss of Laa2 did not disrupt Lft1 localization. Instead, Lft1 puncta were slightly
110 brighter than in wild-type cells (Fig. 2B, C). In addition, Lft1 abundance was unaffected by the loss of

111 Laa2 as detected by immunoblot analysis (Fig. 2D, E). The localization results were surprising because
112 Laa1 localization is strongly affected by the deletion of Laa2 ((Zysnarski et al., 2019) Fig. 3A, B). One
113 possible explanation for this observation is that Lft1 and Laa2 interact with different pools of Laa1. To
114 explore this possibility, we examined the localization of Laa1 in cells lacking Lft1 or Laa2 and in cells
115 lacking both Lft1 and Laa2. We found that the loss of Lft1 alone did not cause a detectable effect on Laa1-
116 GFP localization as monitored by puncta intensity (Fig. 3A, B). As previously reported, the loss of Laa2
117 reduced Laa1-GFP puncta intensity by over one-half (Fig. 3A, B). Notably, simultaneous loss of both Lft1
118 and Laa2 reduced Laa1-GFP puncta intensity to nearly undetectable levels (Fig. 3 A, B). These findings
119 suggest that Laa1 may exist in two populations, one bound to Lft1 and one bound to Laa2. Moreover, it
120 indicates that Laa1 localization depends on these binding partners.

121 To further test whether two populations of Laa1 exist in cells, we asked whether Lft1 and Laa2 interact
122 by co-immunoprecipitation. We were unable to detect an interaction between Lft1 and Laa2 under
123 conditions where both bind to Laa1, indicating that the two form mutually exclusive complexes with Laa1
124 (Fig. 3C). To understand the structural basis of this observation, we predicted complexes between Laa1
125 and Lft1 or Laa2 using AlphaFold2-based structure prediction. Alphafold2 predicted several regions of
126 high-confidence contact between the C-terminus of Laa1 and both Lft1 and Laa2 (Fig. 4A & B,
127 Supplemental data folder 1-6). Surprisingly, despite little sequence similarity (Fig. 4C), the predicted
128 interactions are highly similar (Fig. 4D). Both Lft1 and Laa2 contain several small alpha-helical regions
129 separated by short disordered linkers; these alpha-helical regions interact with an extended interface within
130 the C-terminal 500 amino acids of Laa1. In the predictions, Lft1 binds to Laa1 via four alpha-helical
131 regions (HR 1-4), whereas Laa2 binds to Laa1 via only three (HR1-3). Notably, in the predictions, HR1-
132 3 of Lft1 and Laa2 superimpose almost exactly. This result suggests that Lft1 and Laa2 bind to Laa1 via
133 an overlapping interface and cannot simultaneously bind to Laa1.

134 We validated the interaction interface of Laa1 with Lft1 and Laa2 using Laa1 truncations. We found that
135 both Lft1 and Laa2 bound strongly to a fragment composed of the last 908 amino acids of Laa1 (pGal1-
136 GST-Laa1(1106)), which contains the entire predicted binding domain (Fig. 5A-C). Conversely, neither
137 protein bound to a Laa1 fragment that lacks the terminal 908 amino acids (Laa1(1106)-GST) (Fig. 5 D-F
138). These data indicate that C-terminal 908 amino acids of Laa1 are necessary and sufficient for binding to
139 both Lft1 and Laa2. We next tested truncations that split the predicted binding interface. We found that a
140 fragment composed of the last 304 amino acids of Laa1 (pGAL1-GST-Laa1(1710), which contains the
141 binding interface for HR1 and truncates the binding interface for HR2, failed to bind either Lft1 or Laa2
142 (Fig. 5A-C). Finally, we found that a fragment of Laa1 that lacked the last 304 amino (Laa1(1710)-GST)
143 bound weakly to Lft1, whereas it did not bind Laa2 (Fig. 5 D-F). Notably, this finding is consistent with
144 the more extensive binding interface in the region N-terminal to amino acid 1710 predicted for Lft1
145 (HR3&4) compared to Laa2 (HR3). The concordance of our experimental data with the predicted structure
146 strongly suggests the prediction accurately captures the binding interface on Laa1. Together these results
147 suggest that Lft1 and Laa2 cannot bind Laa1 simultaneously and indicate that Lft1 defines a second Laa1-
148 containing complex in budding yeast.

149 To validate the predicted interface on Lft1, we generated mutations in Lft1 that removed HR1, HR2, and
150 HR3 individually. We found that removing either HR1 or HR2 in Lft1 expressed from its endogenous
151 locus reduced the interaction of Lft1 with Laa1 to about 60% of wild-type levels (Fig. 6A, B). However,
152 removing HR3 reduced the interaction to undetectable levels (Fig. 6A, B). Together these results support
153 the prediction that the Lft1 binding interface is extended and utilizes contacts spanning the region
154 containing HR1-4.

155 Curiously, Lft1-ΔHR2 is 3-fold more abundant than wild-type Lft1, whereas the abundance of Lft1-ΔHR1
156 and Lft1-ΔHR3 is not significantly different from that of wild-type Lft1 (Fig. 6C, D). This finding is

157 surprising because Lft1 is less abundant in cells lacking Laa1 or in cells expressing truncations of Laa1
158 that do not bind Lft1, suggesting that Lft1 is destabilized when it does not bind Laa1. The increased
159 abundance of Lft1-ΔHR2 suggests that HR2 may play a role in destabilizing Lft1 when it is not bound to
160 Laa1.

161 **The Lft1-Laa1 complex does not bind AP1 or control its localization**

162 The only molecular function known for Laa1 is to recruit AP1, a function described for HEATR5 proteins
163 in many other species (Gillard et al., 2015; Le Bras et al., 2012; Yu et al., 2012; Zysnarski et al., 2019).
164 However, HEATR5-proteins are not thought to bind directly to AP1. Instead, they rely on accessory
165 proteins that contain AP1 binding sites that mediate the interaction between the HEATR5 protein and
166 AP1. The AP1 binding site often takes the form of a small peptide motif with the consensus FXXφ (where
167 F is phenylalanine, X is any amino acid, and φ is a hydrophobic residue) in a region rich in acidic amino
168 acids (Duncan et al., 2003; Duncan and Payne, 2003; Mattera et al., 2004). We previously reported that a
169 mutation of the FXXφ in Laa2 eliminated the interaction between Laa1 and AP1 (Zysnarski et al., 2019).
170 However, Lft1 contains one potential AP1 binding motif in its unstructured C-terminus
171 (^{298}DDGDGFEQV), raising the possibility that it too binds AP1. Therefore, we tested whether Lft1 binds
172 AP1. Surprisingly, we were unable to detect an interaction between Lft1 and AP1 using 2-hybrid analysis,
173 or co-immunoprecipitation, suggesting that if Lft1 interacts with AP1, the interaction is weak or depends
174 on other factors that are not recapitulated in our assays (Fig. 7 A-C).

175 To investigate whether the Lft1-Laa1 complex participates in AP1 recruitment, we examined AP1
176 localization in cells lacking Lft1. We found that the loss of Lft1 did not affect AP1 localization as
177 monitored by puncta intensity, and Lft1 did not enhance the AP1 localization defect caused by the loss of
178 Laa2 (Fig. 7 D, E). These results argue that, unlike the Laa2-Laa1 complex, the Lft1-Laa1 complex is not
179 important for recruiting or stabilizing AP1 on membranes. We next asked whether the Lft1-Laa1 complex

180 depends on AP1 for its localization. We found that loss of the AP1 subunit Apl4 elevated Lft1 puncta
181 intensity, similar to the effect of Laa2 (Fig. 2B). The similar effect of *apl2Δ* and *laa2Δ* may indicate that
182 the elevated intensity of Lft1 puncta is due to loss of AP1 function, for example by delaying TGN
183 maturation, rather than competition between Laa2 and Lft1. In any case, these results argue that AP1 does
184 not recruit the Lft1-Laa1 complex to membranes. These findings suggest that Lft1-Laa1 performs at least
185 one function besides recruiting AP1 to membranes.

186 **The Lft1 complex mediates recycling in the TGN**

187 To better understand the function of the Laa1-Lft1 complex, we examined the effect of the loss of Lft1
188 alone or in combination with Laa2 on phenotypes associated with the loss of Laa1. We first examined
189 Sertraline sensitivity. Sertraline is a cationic amphiphilic drug that causes severe growth defects when
190 combined with mutations that impair traffic at the TGN or in the early endosomal system (Rainey et al.,
191 2010). We previously determined that cells lacking Laa1 or Laa2 are sensitive to Sertraline (Zysnarski et
192 al., 2019). However, cells lacking Laa2 were slightly less sensitive than those lacking Laa1.

193 Moreover, in a high throughput study, cells lacking Laa1, Laa2, or Lft1 were all more sensitive to
194 Sertraline than wild-type cells, however, cells lacking Laa1 were far more sensitive than cells lacking
195 either Laa2 or Lft1. When ranked in order of the growth defect caused by *laa1Δ* 12.5 μM Sertraline was
196 ranked 16th out of 4198, whereas *laa2Δ* was the 54th most sensitive, and *lft1Δ* was the 606th most sensitive
197 to Sertraline (Ericson et al., 2008). These differences in sensitivity suggest the Laa2-Laa1 and Lft1-Laa1
198 complex might both contribute to the Sertraline sensitive function of Laa1. To confirm this, we examined
199 the Sertraline sensitivity of cells lacking Laa1, Lft1, Laa2, or a combination of Lft1 and Laa2. Consistent
200 with the prior results, the *laa1Δ* cells were more sensitive than the single deletion of either *LFT1* or *LAA2*
201 as monitored by the IC50 of Sertraline for each of the mutant genotypes (Fig. 8A). Importantly, consistent

202 with the hypothesis that both the Lft1-Laa1 and Laa2-Laa1 complexes contribute to Sertraline sensitivity,
203 the double *lft1Δ laa2Δ* genotype was nearly as sensitive to Sertraline as the *laa1Δ* genotype (Fig. 8A).

204 The growth defect of the double *lft1Δ laa2Δ* mutation in Sertraline suggests that both complexes contribute
205 to Laa1 functions. However, although Sertraline sensitivity is a quantitative metric of defects, the
206 mechanism of Sertraline sensitivity is unclear. Therefore, we examined the effect of Lft1 and Laa2 in
207 traffic at the TGN. To do this, we monitored the localization of Drs2, an aminophospholipid translocase
208 that localizes to the TGN. The TGN in yeast is a maturing compartment. Therefore, the steady-state
209 localization of TGN-resident proteins like Drs2 requires their retrieval from late-stage compartments to
210 early-stage compartments. This 'intra-Golgi' recycling mechanism depends on the clathrin adaptors AP1
211 and Ent5 (Casler et al., 2022). When intra-Golgi recycling is impaired, Drs2 is transported to the plasma
212 membrane. It is then rapidly endocytosed and sorted to the TGN (Liu et al., 2008). Therefore, to visualize
213 defects in Drs2 intra-Golgi recycling, we inhibited endocytosis by treating cells with Latrunculin A as
214 previously described (Liu et al., 2008). Under these conditions, in wild-type cells, a substantial fraction
215 of Drs2 remained localized to the TGN as assessed by co-localization with Sec7 (Fig. 7B). In contrast, in
216 cells lacking either AP1 or Laa1, most of the Drs2 is at the cell surface under these conditions. In cells
217 lacking either Lft1 or Laa2, the phenotype was intermediate (Fig. 7B).

218 To quantify the phenotype, we performed a blinded analysis of whether Drs2 localized to puncta or the
219 plasma membrane in the different samples. In wild-type cells treated with Latrunculin A, approximately
220 60% of the cells were classified as punctate using this analysis. In contrast, in *apl4Δ* or *laa1Δ* cells treated
221 with Latrunculin A, this number was 20% and 15%, respectively (Fig. 7C). Loss of Laa2 alone had little
222 effect on the percent of cells with punctate Drs2 in cells treated with Latrunculin A. In contrast, loss of
223 Lft1 caused a variable outcome. However, in cells lacking both Ltf1 and Laa2, the percent of cells with
224 punctate localization was significantly lower than wild-type and reached a level similar to *laa1Δ* cells.

225 These data suggest that both the Lft1-Laa1 and the Laa2-Laa1 complexes participate in intra-Golgi
226 recycling to maintain Drs2 at the TGN, even though Lft1-Laa1 does not impact AP1 localization.

227 **Human proteins are predicted to bind to Heatr5b via a conserved mechanism.**

228 Although HEATR5 proteins themselves are slowly evolving, their binding partners are fast-evolving
229 (Kuznetsov et al., 2023). For example, clear homologs of Lft1 and Laa2 can be identified only in other
230 fungi (Huerta-Cepas et al., 2019). Similarly, clear homologs to the human Heatr5b binding proteins
231 Aftiphilin and γ-synergin can be identified only in animals (Huerta-Cepas et al., 2019). Since Lft1 and
232 Laa2 bear little sequence similarity yet bind Laa1 in a similar manner, we asked whether other known or
233 suspected HEATR5 binding proteins might share a binding mechanism. To do this, we used AlphaFold2
234 to predict interactions between Heatr5b and its known binding proteins Aftiphilin and γ-synergin, as well
235 as Clba1, an uncharacterized protein with weak similarity to a region of Aftiphilin and Laa2 (Zysnarski et
236 al., 2019). We also predicted interactions between Heatr5a, a paralog of Heatr5b of unknown function.
237 Alphafold2 did not yield high-confidence interactions between Heatr5a or Heatr5b and γ-synergin
238 (Supplemental data folder 7). However, Alphafold2 predicted high-confidence interactions between the
239 C-termini of Heatr5a and Heatr5b and both Aftiphilin and Clba1 (Fig. 9A, Supplemental data folder 8-
240 12). Aftiphilin and Clba1 are predicted to bind over an extended interface in the C-termini of Heatr5a and
241 Heatr5b via three short alpha-helical regions analogous to HR1-3 in Lft1/Laa2. These regions in Aftiphilin
242 and Clba1 have weak but identifiable sequence similarity to one another and to Laa2 (Fig. 9B, (Zysnarski
243 et al., 2019)). Indeed, an area overlapping with HR2 and HR3 has been annotated as the Clba (clathrin
244 binding of Aftiphilin) domain for which Clba1 was named by the HUGO Gene Nomenclature Committee
245 at the European Bioinformatics Institute (Thomas et al., 2022). As with the budding yeast proteins, the
246 human proteins superimpose almost exactly with one another, suggesting that they cannot bind to
247 HEATR5 proteins simultaneously (Fig. 9c). We also compared the predicted interaction surfaces between

248 the budding yeast and human complexes. When aligning the predicted complexes based on the similarity
249 of Laa1 and HEATR5b, we found that Lft1 and Aftiphilin superimposed well, particularly in HR2 and
250 HR3 (Fig. 9d). Together, these results suggest that multiple HEATR5 binding proteins compete for the
251 same interface in both budding yeast and humans and suggest that human HEATR5 proteins may form
252 two or more biochemically distinct complexes.

253 **Discussion**

254 In this study, we report the discovery that the yeast HEATR5 protein, Laa1, participates in two distinct
255 biochemical protein complexes. This is the first report of any HEATR5 protein participating in distinct
256 biochemical complexes with mutually exclusive binding partners. Our discovery challenges previous
257 models for Laa1 functions and introduces the concept that HEATR5 proteins may participate in multiple
258 distinct complexes in other organisms.

259 Our findings indicate that the Lft1-Laa1 and Laa2-Laa1 complexes are at least partially redundant. The
260 source of this redundancy is currently known. Multiple models could explain this redundancy. The two
261 complexes may function interchangeably at the same step (Fig. 10A). Alternately, the two complexes
262 could act in different recycling pathways that emerge from different domains of the TGN or different
263 stages of TGN maturation (Fig. 10B, C). Future work is needed to distinguish these possibilities.

264 Considering our findings that Laa1 performs a function besides recruiting AP1, a re-reading of the prior
265 literature, particularly analysis of high-throughput studies, reveals that other HEATR5 proteins may also
266 have functions besides recruiting AP1. In human cells, knocking down Heatr5b or Aftiphilin causes
267 endocytosed transferrin to accumulate in peripheral endosomes, a phenotype not observed with AP1
268 knockdown (Hirst et al., 2005). In worms, HEATR5, but not AP1, was identified in a screen for genes
269 important for endocytosis (Balklava et al., 2007). In addition, the obligate Heatr5b interaction partners

270 Aftiphilin and γ-synergin were found in the interactome of AP2 and AP3 in human cells, and the plant
271 HEATR5 protein, Sweetie, was found in the interactome of the endocytic T-plate complex (Burman et al.,
272 2005; Dragwidge et al., 2023; Stockhammer et al., 2022). These studies suggest HEATR5 proteins in
273 other organisms have roles outside the AP1 pathway. Whether these additional roles involve two or more
274 distinct HEATR5 complexes remains to be determined.

275 This study also defines the common molecular binding interface between the yeast HEATR5 protein and
276 its co-factors using high-confidence structure predictions and biochemical analyses. Notably, we report
277 high-confidence predictions of the human proteins binding Aftiphilin and Clab1, which are highly similar
278 to the experimentally verified interface in the yeast proteins. Although the interactions between Aftiphilin
279 and Heatr5a and Clba1 and Heatr5a or Heatr5b have yet to be experimentally verified, the concordance
280 of the predicted interaction interfaces with the experimentally verified yeast interaction interfaces suggests
281 the predicted interfaces likely reflect the native situation.

282 The interaction between Laa1 and Lft1, and Laa2 is stable enough to be maintained during
283 immunoprecipitations (Fig. 2,(Zysnarski et al., 2019)). However, it remains unclear how stable the
284 interactions are in vivo. Laa1 binding protects both wild-type Lft1 and Laa2 from degradation, as seen by
285 the lower abundances of both in cells lacking Laa1 (Fig. 2,(Zysnarski et al., 2019)). This lower abundance
286 argues that if Lft1-Laa1 and Laa2-Laa1 complexes dynamically assemble and disassemble, free Lft1 and
287 Laa2 are likely short-lived either because the released protein is rapidly bound to a new Laa1 molecule or
288 degraded. Notably, Lft1 and Laa2 have different degradation kinetics. In a genome-wide analysis of
289 protein stability, Laa2 has a half-life of 10.1 hours, similar to the half-life of Laa1 (10.5 hr) and the bulk
290 of the budding yeast proteome (>8 hr), whose abundance is regulated by synthesis rate rather than
291 degradation rate (Christiano et al., 2014). This half-life is consistent with Laa2 either binding stably to
292 Laa1 or rapidly rebinding such that Laa2 is not actively degraded even if it engages in dynamic assembly

293 cycles. In contrast, Lft1 has a half-life of 5.7 hours, placing it in the 15% budding yeast proteome
294 specifically targeted by degradation pathways. Future work will be needed to assess whether Lft1-Laa1
295 or Laa2-Laa1 complexes assemble and disassemble dynamically in vivo and, if so, whether targeted
296 degradation of Lft1 plays a vital role under normal conditions.

297 The extended nature of the Laa1 binding site on Lft1 and Laa2 may be significant for their molecular
298 mechanism. The Lft1 and Laa2 binding sites for Laa1 are composed of a series of alpha-helical regions
299 separated by unstructured segments (Fig. 4). Our studies using truncations of Laa1 and HR deletion
300 mutations of Lft1 indicate that multiple areas of this extended interface contribute to the binding
301 mechanism (Fig. 5, 6). We speculate that this interface may allow Lft1 and Laa2 to remain bound to Laa1
302 even if the conformation of Laa1 changes. Based on its predicted structure, Laa1 is likely to be
303 conformationally dynamic. The predicted C-terminus of Laa1 is almost entirely tandem HEAT repeats.
304 The HEAT repeat is a simple fold composed of two alpha helices separated by a short linker. This
305 arrangement is common in biology. Tandem HEAT repeats appear in diverse proteins, including kinases,
306 importins, transcription factors, and vesicular coat proteins (Kobe et al., 1999). In these proteins, the
307 tandem HEAT repeats form an alpha-solenoid that can display an extraordinary level of conformational
308 flexibility, in some cases elastically stretching by 2-fold (Forwood et al., 2010; Kappel et al., 2010;
309 Yoshimura and Hirano, 2016). In addition, Laa1 contains an unstructured loop between amino acids 1711-
310 1733, which lies near the binding sites for HR2 on Lft1 and Laa2. If Laa1 undergoes elastic stretching or
311 other conformational changes, the extended binding interface may play a role in maintaining the
312 interaction between Laa1 and its binding partners.

313 In summary, these findings reveal that Laa1 participates in two biochemically distinct complexes. The
314 complexes are defined by the mutually exclusive binding of two fast-evolving binding partners. The
315 binding mechanism is characterized by an extended surface on both Laa1 and its binding partners. Overall,

316 the binding mechanism may provide a paradigm for HEATR5 binding proteins in many organisms. The
317 two Laa1 complexes function at least partially redundantly in intra-Golgi recycling, however, their exact
318 mechanistic function remains unknown. Given the large size of Laa1, there are likely additional protein-
319 protein or protein-lipid interactions mediated by Laa1 that remain undiscovered. Future studies are needed
320 to elucidate these additional interactions and reveal a complete picture of the molecular mechanism of
321 Laa1 function in membrane traffic in budding yeast.

322 **Materials and Methods**

323 The strains, plasmids, and oligonucleotides used for this study are listed in Tables 1-3 (James et al., 1996;
324 Noguchi et al., 2008; Plemel et al., 2021). pFA6A-mcherry::His6Mx was generated by replacing GFP in
325 pFA6a-GFP::His6Mx with mCherry from pRSETB-mcherry (Shaner et al., 2004). pMD397(pGAD-C1-
326 Lft1) and pMD380 (pGEX4T1-Lft1) was generated by amplifying *LFT1* from genomic DNA using
327 oligonucleotides FJ064 and FL065 and subcloning into pGADC1 between the BamHI and SalI sites.
328 pMD394-396 were generated by amplifying from pMD380 with oligo pairs described in Table 3 and using
329 3-piece assembly reactions to generate the deletion alleles (Gibson et al., 2009). Tags and deletions were
330 integrated into the genome using a one-step PCR-based method (Longtine et al., 1998; Noguchi et al.,
331 2008). Mutations in *LFT1* were generated by a two-piece PCR-mediated gene replacement strategy, the
332 *LFT1* wild-type or mutant open reading frames were amplified from pMD380 and pMD394-pMD396
333 using oligonucleotides MD1258 and MD1259 for wild-type and all mutations except the deletion of helix
334 1 which was amplified with MD1269b and MD1259. The open reading frame fragment was co-
335 transformed with a fragment amplified from pFA6a-6His-TEV-Flag-His6Mx using MD902 and MD904
336 into cells carrying a deletion of *LFT1.* Combinations of tags, mutations, and deletions were performed
337 using manual tetrad dissection. Yeast cells were grown in yeast/peptone medium supplemented with 2%
338 glucose and a mixture of adenine, uracil, and tryptophan (YPD+AUT), or yeast/peptone medium

339 supplemented with 2% galactose and a mixture of adenine, uracil, and tryptophan (YPG+AUT) or
340 synthetic medium SD supplemented with 2% glucose and an amino acid mix as previously described
341 (Lang et al., 2014). Sertraline was from Fisher Scientific. Sertraline (10 mm) was prepared in DMSO.
342 FM4-64 (SnaptoRed C2) was prepared in DMSO. Antibodies against Myc (9E10, RRID:CVCL_L708)
343 were from Biolegend, PGK1 (22C5D8,RRID:AB_2532235) was from Novex, HA (12CA5,
344 RRID:AB_514505) and Flag (M2, RRID:AB_439685) were from Sigma. GST-antibody was described
345 previously (Hung et al., 2012). Alexa Fluor 647-conjugated goat anti-mouse (RRID:AB_141698) and
346 Alexa Fluor 647 goat anti-rabbit (RRID:AB_141663) antibody were from Life Technologies.

347 Graphs were generated and statistical analysis was performed with GraphPad Prism v7.00-9.00 (GraphPad
348 Software, La Jolla, CA).

349 Imaging and analysis was performed as described previously (Hung and Duncan, 2016). Briefly, unless
350 indicated otherwise cells were cultured to logarithmic phase in SD medium, centrifuged briefly, and
351 mounted on an uncoated coverslip in growth medium. Images were collected with a Nikon Ti-E inverted
352 microscope with a 1.4 numerical aperture/100× oil immersion objective. The Lumencor LED light engine
353 (472/20 nm for GFP and 575/20 nm for mCherry) was used for fluorophore excitation. Filters were
354 ET/GFP-mCherry (59,002×), excitation dichroic (89019bs), and emission-side dichroic (T560lpxr), and
355 for emission filters, ET525/50 m and ET595/50 m(Chroma).

356 The intensity of fluorescence puncta in cells was quantified as previously described (Martinez-Marquez
357 and Duncan, 2018). Z-stack images were first compressed to a single maximum-intensity image using
358 ImageJ. The resulting image was denoised using the "Denoise image" menu from the SpatTrackV2
359 software (Lund et al., 2014). Image analysis was performed in ImageJ. To define regions of GFP
360 localization, the denoised image was thresholded using Otsu's method with ImageJ with the stacked
361 histogram option selected. GFP positive regions of interest were defined using the "Analyze Particles"

362 menu from ImageJ on the binary thresholded image. The GFP-positive regions of interest were then used
363 to measure fluorescence intensity from a background subtracted Z-stack compressed but non-denoised
364 image. Fluorescence intensity was determined from at least eight fields of view per sample, each
365 containing at least five cells. Experiments were repeated as indicated in the figures using at least two
366 different strains for the same genotype.

367 For co-localization analysis, GFP and mCherry positive regions of interest were defined using the same
368 process used for puncta intensity analysis. GFP structures that contain mCherry, were defined as structures
369 for which at least 30% of the GFP positive area of the structure was also mCherry positive and vice versa
370 for mCherry structures that contain GFP. At least eight fields of view were analyzed per sample, each
371 containing at least five cells. Experiments were repeated as indicated in the figures using two different
372 strains for each genotype.

373 For Drs2 localization, cells were transferred to a tube roller at 25C at least 3 hours before treating with 76
374 µg/ml Latrunculin or 2% DMSO. Cells were incubated for 30 min at 25C in microfuge tubes with
375 punctured lids in a shaking heating block, before images were collected. Z-stack images were first
376 compressed to a single maximum-intensity image using ImageJ. Files were copied and renamed to obscure
377 genotype information and cells were manually scored as having punctate or cell surface localization. At
378 least five fields of view were analyzed per sample, each containing at least five cells.

379 FM4-64 staining of yeast vacuoles was performed as previously described (Buelto et al., 2020).

380 For immunoblotting, after SDS-PAGE, samples were transferred to nitrocellulose, blocked with 5% milk
381 in TBS-T (137 mm NaCl, 15.2 mm Tris-HCl, 4.54 mm Tris, 0.896 mm Tween 20), and then probed with
382 primary and fluorescent secondary antibodies. Fluorescence signals were detected on an Azure 600
383 imaging system (Azure Biosciences). Image analysis was performed in ImageJ.

384 Whole-cell yeast extracts for protein abundance assessment were generated using glass bead lysis in SDS
385 sample buffer as previously described (Aoh et al., 2011). Cell lysates for immunoprecipitation and GST-
386 pulldowns were generated by glass-bead lysis in HEKG5 (20 mm Hepes, pH 7.5, 1 mm EDTA, 150 mm
387 KCl, 5% glycerol) with protease inhibitor mixture without EDTA (Promega), followed by the addition of
388 0.3% CHAPS. The lysates were clarified by centrifugation at 13,000 rpm for 10 min at 4 °C. Protein
389 concentrations were determined using Biorad Protein Assay (Biorad) and protein concentrations were
390 adjusted to 2ml in 500 µl HEKG5. For Flag-IP, 6 µls of EZview™ Red ANTI-FLAG® M2 Affinity Gel
391 (Sigma). For GST-pull downs, 20µls 50% Glutathione agarose (G-Biosciences) was added. For myc-IP,
392 20 µls 20% Protein A Sepharose (Cytvia) and 0.5 anti-myc antibodies were added. The lysates were
393 incubated two hours at 4 °C. For immunoprecipitations, the beads were washed three times with ice-cold
394 HEKG5 with 0.3% CHAPS, and the bound proteins were eluted with SDS sample buffer. For GST-
395 pulldowns, the beads were wash twice with HEKG5 with 0.3% CHAPS and once with HEKG5 without
396 CHAPS. The beads were resuspended in 50 µl 100 mm Tris, pH 9, 200 mm NaCl, 5 mm DTT, 20 mm
397 reduced GSH, and incubated for 10 min at room temperature. The supernatants were reserved. A second
398 elution was then performed the two supernatants were combined. For all samples, cells were cultured to
399 mid-log phase in YPD+AUT except for samples described in Figure 6 A and Figure 7 A which were
400 grown in YPG+AUT.

401 Two-hybrid interactions were monitored as previously described (Duncan et al., 2003).

402 IC50 values were determined as previously described (Hung et al., 2018).

403 Structure predictions were performed using alphafold2_multimer_v3 version 1.5.2 with the following
404 settings: mas_mode mmseqs2_uniref_env, 5 models, 6 recycles, 1 ensemble (Mirdita et al., 2022)

405 Structure comparisons and alignments were performed in UCSF ChimeraX version 1.4 with the following
406 settings: Sequence alignment algorithm Needleman-Wunsch, Matrix Blosum-62, Gap extension penalty
407 1, iterate by pruning long atom pairs was selected and cutoff distance was set at 2 (Goddard et al., 2018;
408 Pettersen et al., 2021).

409 Tables of strains, plasmids, and oligonucleotides used are available as supplemental documents. Structure
410 predictions and accompanying documents are available as supplemental materials.

411 **Acknowledgements**

412 UCSF ChimeraX was developed by the Resource for Biocomputing, Visualization, and Informatics at the
413 University of California, San Francisco, with support from National Institutes of Health R01-GM129325
414 and the Office of Cyber Infrastructure and Computational Biology, National Institute of Allergy and
415 Infectious Diseases.

416 This work was supported by the National Institutes of Health (R01-GM129255, UL1-TR002240).
417 Microscopy was performed on a system generously provided by Ajit P. Joglekar. We thank Ming Li,
418 Yanzhuang Wang and Ajit Joglekar for helpful comments on this manuscript.

419 Author contributions: L.J. Marmorale, H. Jin, T. Reidy, and M.C. Duncan conceived of the experiments.
420 L.J. Marmorale, H. Jin, T. Reidy, C. Zysnarski, F. Jordan-Javed, and S. Lahiri generated the reagents. L.J.
421 Marmorale, H. Jin, T. Reidy, C. Zysnarski, B. Palomino-Alonso, and M.C. Duncan performed the
422 experiments and analyzed the data. M.C. Duncan wrote the manuscript and secured funding.

423

424

425

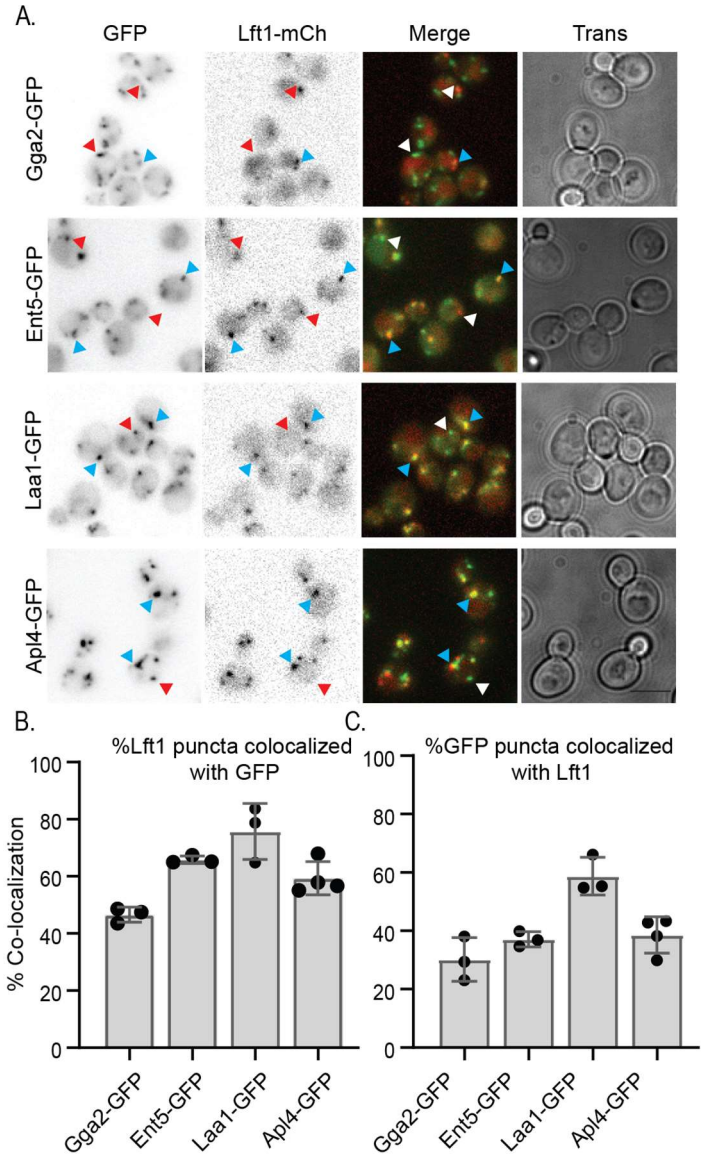

Figure 1. Lft1 shows a high level of co-localization with Laa1. A. Indicated gene fusions were expressed from their endogenous loci and cells were imaged as described in the materials and methods. Scale bar is 5 µm. Blue arrowheads indicate regions of co-localization. Red/White arroweads indicate regions where co-localization was not observed. B. Percent of Lft1 structures that contained indicated GFP protein and C. Percent of structures labeled with indicated GFP-protein that contained Lft1 were determined as described in materials and methods. Charts show percentages from individual replicates, error bars indicate standard deviation.

427

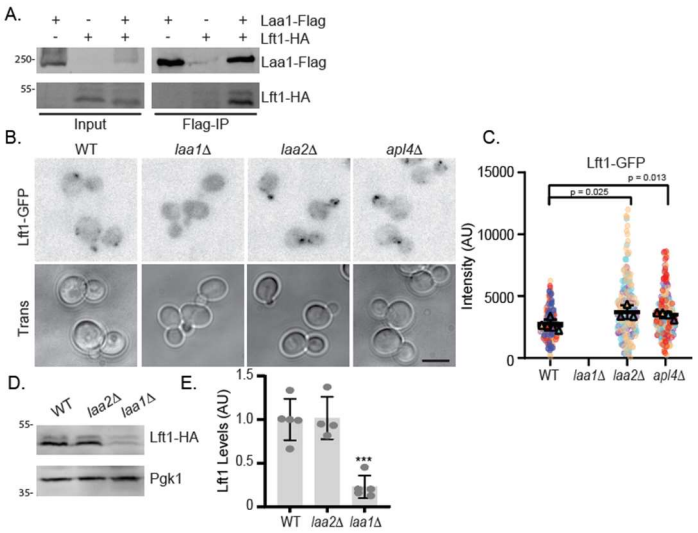

Figure 2. Lft1 binds Laa1 and depends on Laa1 for protein stability. A. Lft1 binds Laa1 as detected by immunoprecipitation. Flag-tagged proteins were immunoprecipitated from cells expressing indicated gene fusions expressed from their endogenous loci and probed for Flag and HA. B. Lft1-GFP is not detectable in cells lacking Laa1. Cells with indicated genotypes were imaged as described in materials and methods. Scale bar is 5 µm C. Quantification of Lft1 puncta intensity in indicated cells. Charts show super-plots of mean values from replicate experiments plotted over individual intensity measurements which are color coded for each replicate experiment. The standard deviations of the mean values are shown. P-values derive from unpaired T-tests of the mean values of replicate experiments D. Lft1 is abundance is lower in cells lacking Laa1 but not Laa2. Lysates of cells of indicated genotypes were probed for HA or PGK1, used as a lysis control. E. Charts of intensity values from D. The standard deviations are shown. P-values derive from Dunnett's multiple comparisons test. Chart shows standard deviations.

428

429

430

431

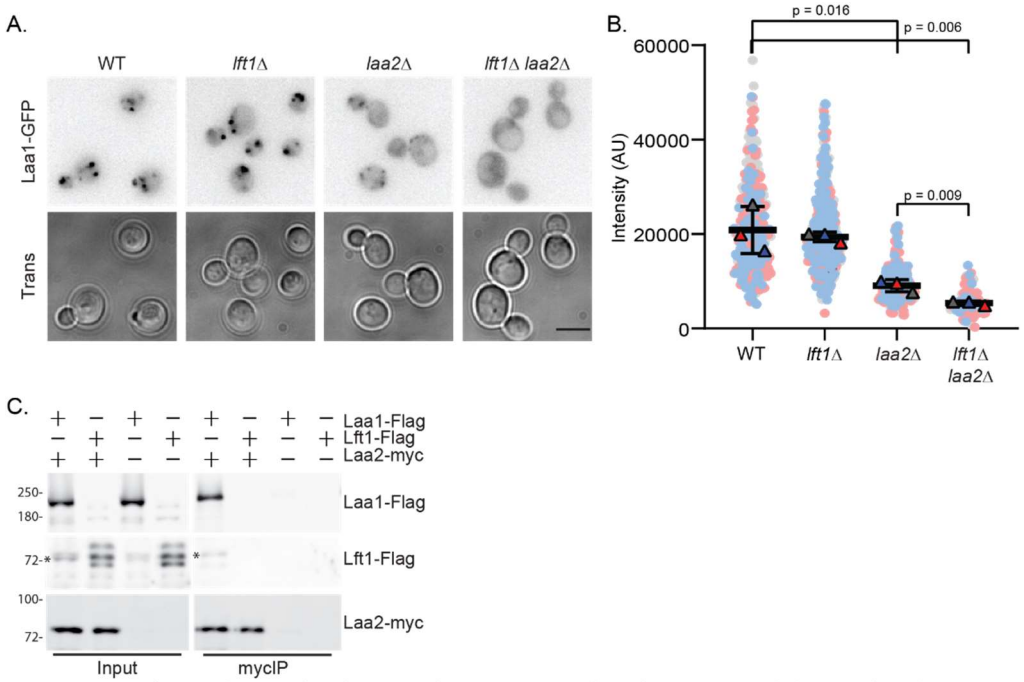

Figure 3. Lft1 and Laa2 both contribute to Laa1 localization and do not bind to one another. A. Cells with indicated genotypes were imaged as described in materials and methods. Scale bar is 5 µm B. Quantification of puncta intensity as described in Fig. 2C. C. Laa2 does not bind Lft1 as detected by immunoprecipitation. Myc-tagged proteins were immunoprecipitated from cells expressing indicated gene fusions from their endogenous loci and probed for myc and Flag. * indicates a degradation product from Laa1 migrating near the size of Lft1. Lft1-Flag migrates as a triplet under the conditions used for the myc IP

432

433

434

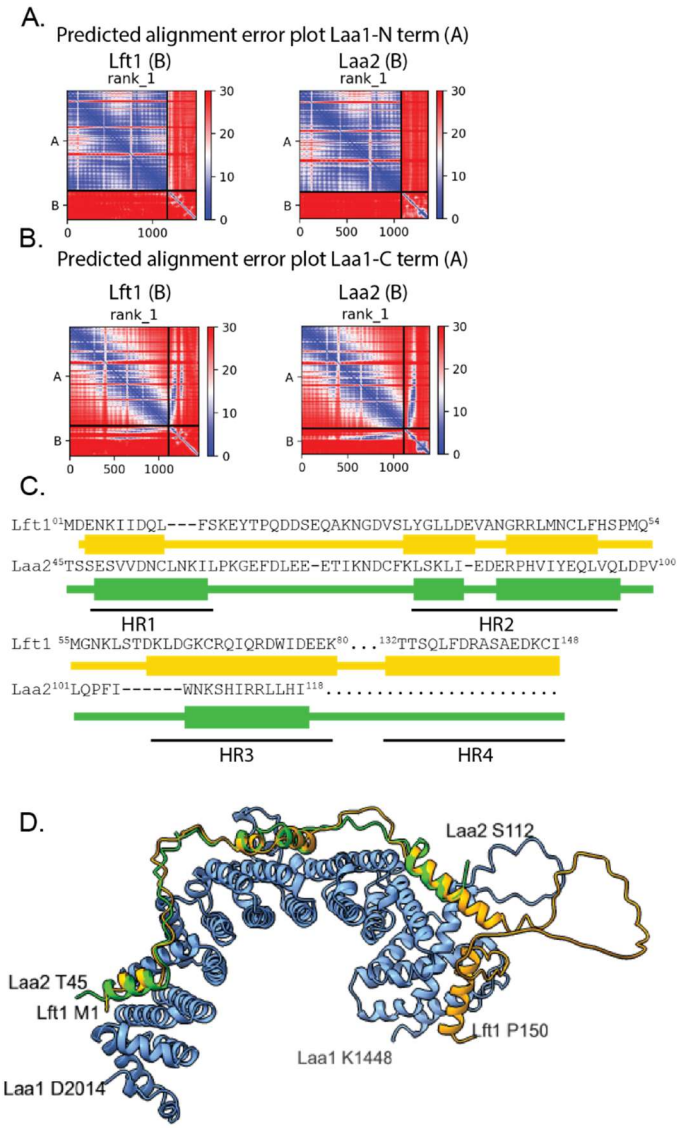

Figure 4. Lft1 and Laa2 are predicted to bind to an overlapping interface on the Laa1 C-terminus. A. No high-confidence interactions are predicted between the N-terminus of Laa1 and either Lft1 or Laa2, suggesting neither protein interacts with the N-terminus. Graphs show predicted alignment error for the top models of alpha fold prediction of dimer. Blue indicates the highest confidence. B. High confidence interactions are predicted between the C-terminus of Laa1 and both Lft1 or Laa2, suggesting both proteins interact with the C-terminus. Graphs as in A. C. Lft1 and Laa2 bear little sequence identity in predicted Laa1 interacting regions. The illustration shows sequence alignment of Lft1 and Laa2 based on overlay generated with ChimeraX matchmaker tool aligning the Laa1 C-terminus from the predicted dimeric structures. Helixes are indicated as boxes. The helical regions (HR) 1-4 are indicated below. D. Lft1 and Laa2 are predicted to adopt a similar fold when binding to Laa1. Illustration shows overlay of predicted structures described in C. Lft1 is orange, and Laa2 is green. Laa1 is in blue, the last 304 amino acids are indicated in a darker blue.

435

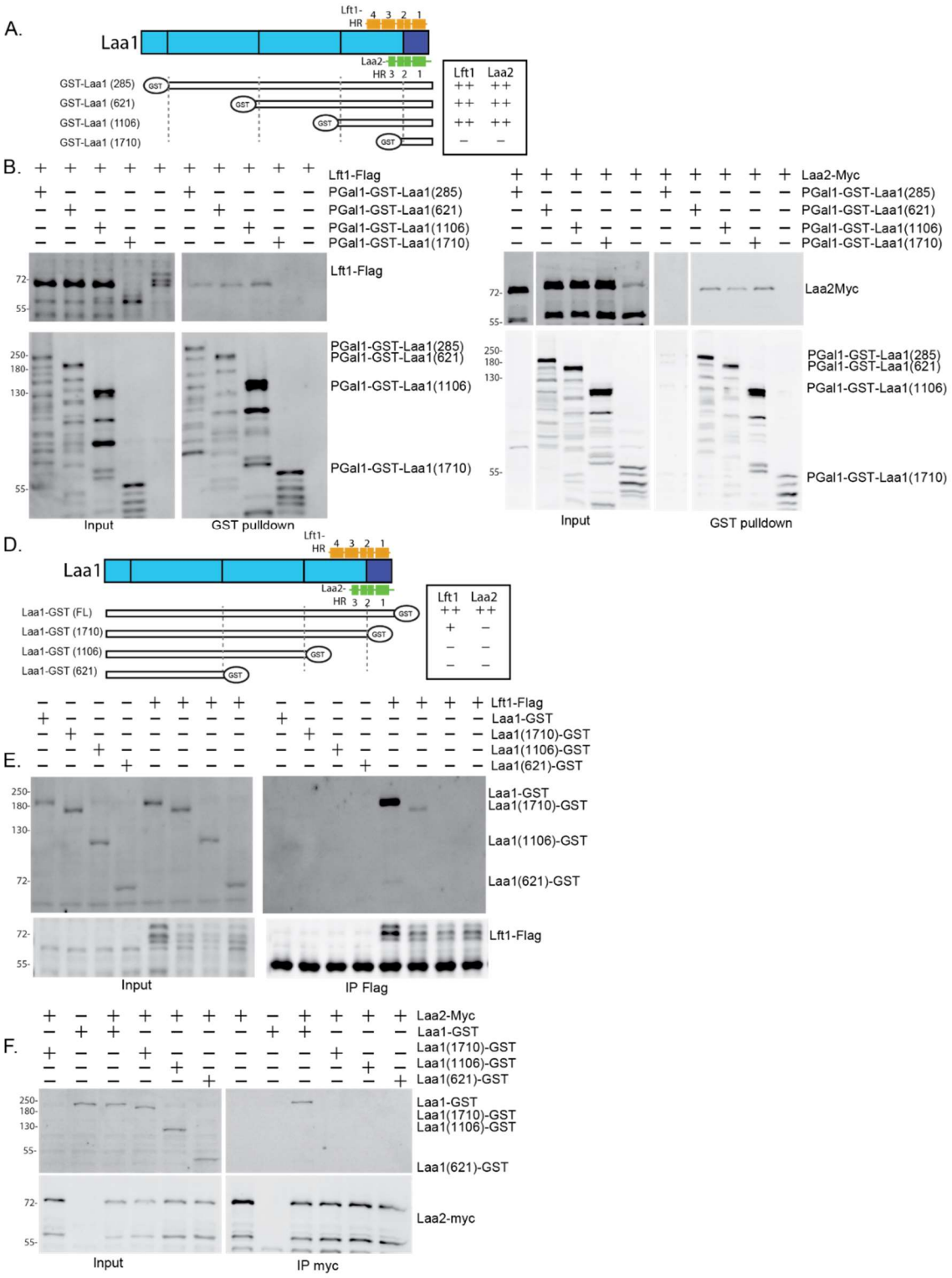

Figure 5. Lft1 and Laa2 bind to the C-terminus of Laa1. (cont)

436

Figure 5. Lft1 and Laa2 bind to the C-terminus of Laa1. A. Schematic of Laa1 fragments used in B and C, and approximate orientation to Lft1 and Laa2 HRs. Strength of binding to Lft1 and Laa2 is indicated to the right. B & C Lft1 and Laa2 bind to Laa1 fragments that encompass the last 908 amino acids of Laa1 (pGAL1-GST-Laa1(1106). GST-tagged proteins were isolated using Glutathione beads from cells expressing indicated gene fusions expressed from their endogenous loci and probed for GST and Flag or Myc. Note that Lft1-Flag migrates as a single band under conditions where Laa1 is overexpressed and can bind Lft1, it migrates as a triplet when Laa1 is not overexpressed. D. Schematic of Laa1 fragments used in E and F and approximate orientation to Lft1 and Laa2 HRs. Strength of binding to Lft1 and Laa2 is indicated to the right. E. Lft1 binds weakly to Laa1 missing the last 304 amino acids (Laa1(1710)-GST), but not larger deletions. Flag-tagged proteins were immunoprecipitated from cells expressing indicated gene fusions expressed from their endogenous loci and probed for GST and Flag. F. Lft1 Laa2 does not bind to any C-terminal truncations tested. Myc-tagged proteins were immunoprecipitated from cells expressing indicated gene fusions expressed from their endogenous loci and probed for GST and myc.

437

438

439

440

441

442

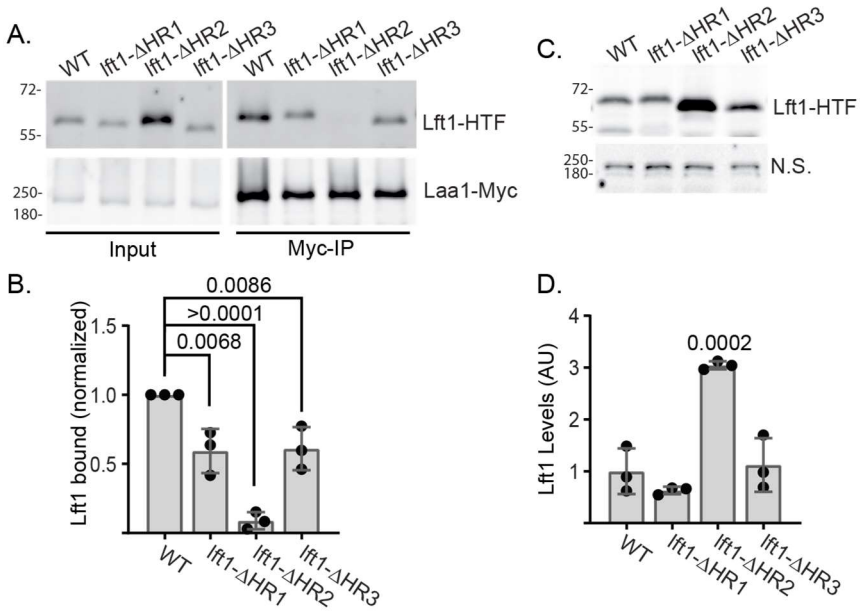

Figure 6. Multiple Lft1 helical regions contribute to binding. A. Indicated *LFT1* mutations were tagged with 6-HIS-TEV-3FLAG (HTF) and expressed from the endogenous locus in cells expressing Laa1-myc from the endogenous locus. Myc-tagged proteins were immunoprecipitated and probed for Myc and Flag B. Lft1 bound was quantified. Lft1 signal was normalized to the amount of Laa1 in each sample and then to the normalized signal for wild-type reactions on the same immunoblot. C. lft1-ΔHR2 is more abundant than wild-type Lft1. Lysates from strains described in A were generated and immunoblotted for Flag. Equal loading was confirmed with an endogenous protein that cross-reacts with the flag antibody (N.S.) D. Lft1 abundance was quantified. Signal intensity was normalized to the average of the wild-type signal. P-values derive from Dunnett's multiple comparisons test. Charts show standard deviations.

443

444

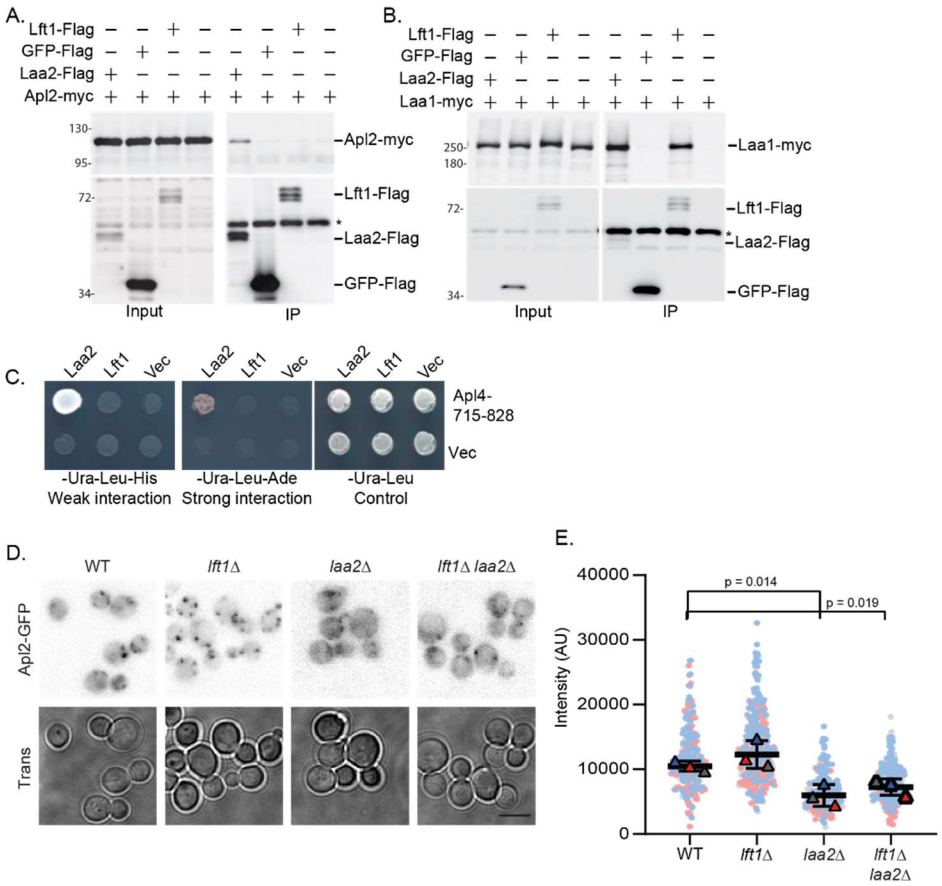

Figure 7. Lft1 does not detectably bind to AP1 or contribute to its localization. A. AP1 was not detected in coimmunoprecipitation samples with Lft1 under conditions where Laa2 binds AP1 and B. under conditions where Lft1 binds Laa1. Myc-tagged proteins were immunoprecipitated from cells expressing indicated gene fusions expressed from their endogenous loci and probed for Myc and Flag. *indicates antibody band. C. An interaction between Lft1 and AP1-γ ear (Apl4-a.a.715-828) was not detected by 2-hybrid under conditions where AP1- γ ear bind Laa2. D. Loss of Lft1 does not impact AP1 localization. Cells with indicated genotypes were imaged as described in materials and methods. Scale bar is 5 µm E. Quantification of puncta intensity as described in Fig. 2C.

445

446

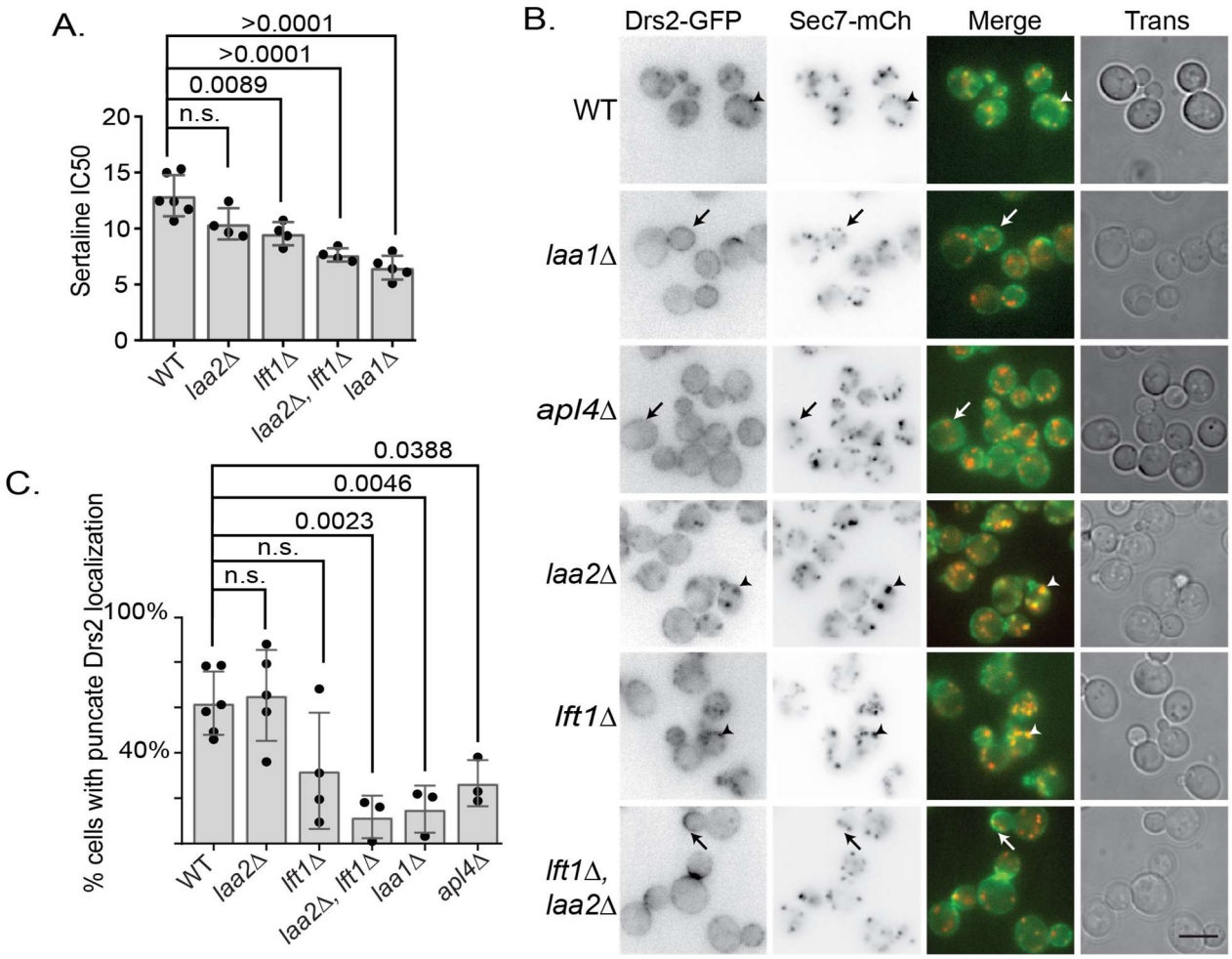

Figure 8. The Lft1-Laa1 and Laa2-Lft1 complexes both mediate intra-Golgi recycling. A. Cells lacking both Lft1 and Laa2 are sensitive to Sertraline at levels similar to cells lacking Laa1. Charts show IC50 values from replicate experiments and standard deviations. P-values are from a student t-test.
B. Cells lacking both Lft1 and Laa2 are severely defective in Drs2 recycling. Drs2 recycling was monitored. Cells with defective recycling accumulate Drs2 at the cell surface after latrunculin A treatment (arrows), whereas those with normal recycling have Drs2 in Sec7-positive puncta (arrowheads) C. Quantification cells with punctate Drs2 localization as described in the materials and methods. Charts show percent of cells scored as having defects in Drs2 localization from replicate experiments and standard deviations. P-values are from a student t-test. Scale bar is 5 µm.

447

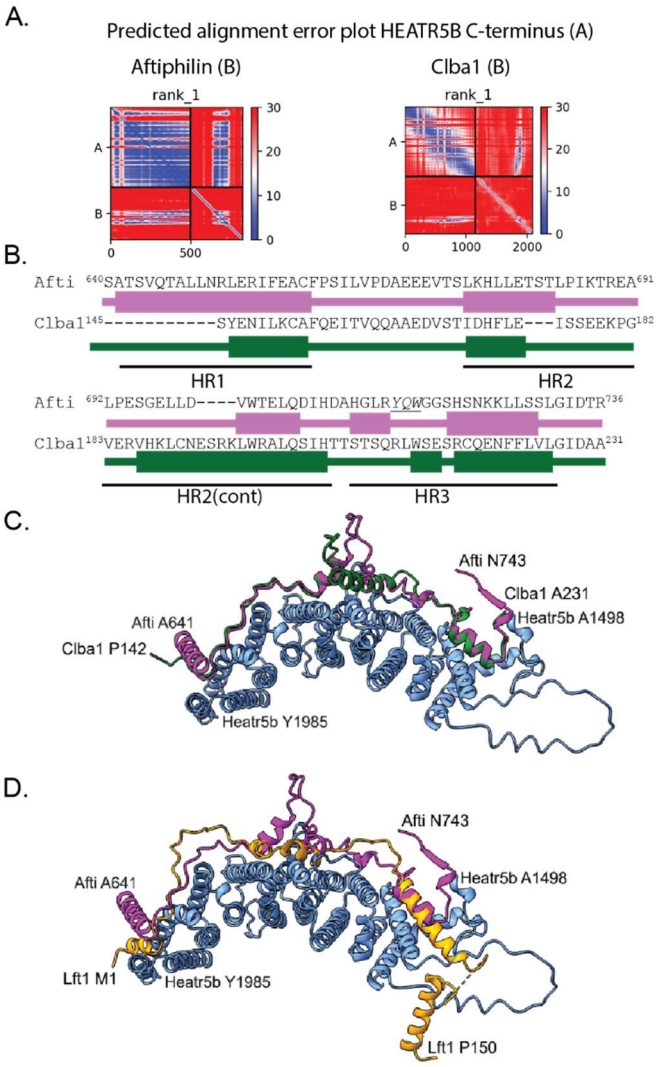

Figure 9. Human proteins are predicted to bind an overlapping interface in the c-terminus of Heatr5b similar to the Laa1-Lft1/Laa2 binding interface. A. High confidence interactions are predicted between the C-terminus of Heatr5b and aftiphilin and Clba1. Charts are as described in Figure 4. B. Aftifphilin and Clba1 display weak similarity in the predicted Heatr5 interacting regions. Diagrams are as described in Figure 4, based on matchmaker tool aligning Aftiphilin and Clba1 in the predicted structures. C. Aftilphilin and Clba1 are predicted to adopt a similar fold and interact with the same regions of Heatr5b. Illustration shows structure alignment as described in panel B. D. Aftiphilin and Lft1 are predicted to bind HEATR5 proteins via a related interface. Illustration shows structure alignment based on matchmaker tool aligning Laa1 and HEATR5b. Laa1/HEATR5b are in blue, Aftiphilin is in magenta, Clba1 is in dark green and Lft1 is in orange

448

449

450

451

452

453

454

455

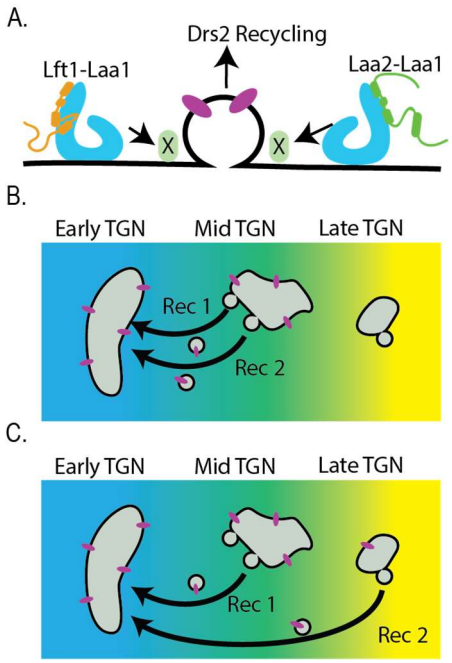

Figure 10. Models of potential roles of Lft1-Laa1 and Laa2-Laa1 complexes in intra-Golgi recycling. A. The two complexes redundantly perform an activity needed to recycle Drs2 from a late-stage TGN to an early-stage TGN. B and C. The two complexes act in two different pathways (Rec 1 and Rec 2) that emerge from different domains of the TGN (B) or that act on sequential stages of TGN maturation (C). Drs2 can recycle by either pathway. When both are disrupted Drs2 is transported to the cell surface.

Aoh, Q.L., L.M. Graves, and M.C. Duncan. 2011. Glucose regulates clathrin adaptors at the trans-Golgi network and endosomes. *Mol Biol Cell*. 22:3671-3683.
Balklava, Z., S. Pant, H. Fares, and B.D. Grant. 2007. Genome-wide analysis identifies a general requirement for polarity proteins in endocytic traffic. *Nat Cell Biol*. 9:1066-1073.
Buelto, D., C.W. Hung, Q.L. Aoh, S. Lahiri, and M.C. Duncan. 2020. Plasma membrane to vacuole traffic induced by glucose starvation requires Gga2-dependent sorting at the trans-Golgi network. *Biol Cell*. 112:349-367.
Burman, J.L., S. Wasiak, B. Ritter, E. de Heuvel, and P.S. McPherson. 2005. Aftiphilin is a component of the clathrin machinery in neurons. *FEBS Lett*. 579:2177-2184.
Casler, J.C., N. Johnson, A.H. Krahn, A. Pantazopoulou, K.J. Day, and B.S. Glick. 2022. Clathrin adaptors mediate two sequential pathways of intra-Golgi recycling. *J Cell Biol*. 221.
Casler, J.C., E. Papanikou, J.J. Barrero, and B.S. Glick. 2019. Maturation-driven transport and AP-1-dependent recycling of a secretory cargo in the Golgi. *J Cell Biol*. 218:1582-1601.
Christiano, R., N. Nagaraj, F. Frohlich, and T.C. Walther. 2014. Global proteome turnover analyses of the Yeasts S. cerevisiae and S. pombe. *Cell Rep*. 9:1959-1965.
Daboussi, L., G. Costaguta, and G.S. Payne. 2012. Phosphoinositide-mediated clathrin adaptor progression at the trans-Golgi network. *Nat Cell Biol*. 14:239-248.
Dragwidge, J.M., Y. Wang, L. Brocard, A.D. Meyer, R. Hudeček, D. Eeckhout, P. Grones, M. Buridan, C. Chambaud, P. Pejchar, M. Potocký, J. Winkler, M. Vandorpe, N. Serre, M. Fendrych, A. Bernard, G.D. Jaeger, R. Pleskot, X. Fang, and D.V. Damme. 2023. Biomolecular condensation orchestrates clathrin-mediated endocytosis in plants. *bioRxiv*:2022.2003.2017.484738.
Duncan, M.C. 2022. New directions for the clathrin adaptor AP-1 in cell biology and human disease. *Curr Opin Cell Biol*. 76:102079.
Duncan, M.C., G. Costaguta, and G.S. Payne. 2003. Yeast epsin-related proteins required for Golgi-endosome traffic define a gamma-adaptin ear-binding motif. *Nat Cell Biol*. 5:77-81.
Duncan, M.C., and G.S. Payne. 2003. ENTH/ANTH domains expand to the Golgi. *Trends Cell Biol*. 13:211-215.
Ericson, E., M. Gebbia, L.E. Heisler, J. Wildenhain, M. Tyers, G. Giaever, and C. Nislow. 2008. Off-target effects of psychoactive drugs revealed by genome-wide assays in yeast. *PLoS Genet*. 4:e1000151.
Fernandez, G.E., and G.S. Payne. 2006. Laa1p, a conserved AP-1 accessory protein important for AP-1 localization in yeast. *Mol Biol Cell*. 17:3304-3317.
Forwood, J.K., A. Lange, U. Zachariae, M. Marfori, C. Preast, H. Grubmuller, M. Stewart, A.H. Corbett, and B. Kobe. 2010. Quantitative structural analysis of importin-beta flexibility: paradigm for solenoid protein structures. *Structure*. 18:1171-1183.
Ghosh, S.G., M.W. Breuss, Z. Schlachetzki, G. Chai, D. Ross, V. Stanley, F.M. Sonmez, H. Topaloglu, M.S. Zaki, H. Hosny, S. Gad, and J.G. Gleeson. 2021. Biallelic hypomorphic mutations in HEATR5B, encoding HEAT repeat-containing protein 5B, in a neurological syndrome with pontocerebellar hypoplasia. *Eur J Hum Genet*. 29:957-964.
Gibson, D.G., L. Young, R.Y. Chuang, J.C. Venter, C.A. Hutchison, and H.O. Smith. 2009. Enzymatic assembly of DNA molecules up to several hundred kilobases. *Nature Methods*. 6:343-U341.
Gillard, G., M. Shafaq-Zadah, O. Nicolle, R. Damaj, J. Pecreaux, and G. Michaux. 2015. Control of E-cadherin apical localisation and morphogenesis by a SOAP-1/AP-1/clathrin pathway in C. elegans epidermal cells. *Development*. 142:1684-1694.
Goddard, T.D., C.C. Huang, E.C. Meng, E.F. Pettersen, G.S. Couch, J.H. Morris, and T.E. Ferrin. 2018. UCSF ChimeraX: Meeting modern challenges in visualization and analysis. *Protein Sci*. 27:14-25.
Highland, C.M., and J.C. Fromme. 2021. Arf1 directly recruits the Pik1-Frq1 PI4K complex to regulate the final stages of Golgi maturation. *Mol Biol Cell*. 32:1064-1080.
Hirst, J., G.H. Borner, M. Harbour, and M.S. Robinson. 2005. The aftiphilin/p200/gamma-synergin complex. *Mol Biol Cell*. 16:2554-2565.

504 Huerta-Cepas, J., D. Szklarczyk, D. Heller, A. Hernandez-Plaza, S.K. Forslund, H. Cook, D.R. Mende, I. Letunic,
505 T. Rattei, L.J. Jensen, C. von Mering, and P. Bork. 2019. eggNOG 5.0: a hierarchical, functionally and
506 phylogenetically annotated orthology resource based on 5090 organisms and 2502 viruses. *Nucleic Acids*
507 *Res*. 47:D309-D314.
508 Huh, W.K., J.V. Falvo, L.C. Gerke, A.S. Carroll, R.W. Howson, J.S. Weissman, and E.K. O'Shea. 2003. Global
509 analysis of protein localization in budding yeast. *Nature*. 425:686-691.
510 Hung, C.W., and M.C. Duncan. 2016. Clathrin binding by the adaptor Ent5 promotes late stages of clathrin coat
511 maturation. *Mol Biol Cell*. 27:1143-1153.
512 Hung, C.W., J.Y. Martinez-Marquez, F.T. Javed, and M.C. Duncan. 2018. A simple and inexpensive quantitative
513 technique for determining chemical sensitivity in Saccharomyces cerevisiae. *Sci Rep*. 8:11919.
514 James, P., J. Halladay, and E.A. Craig. 1996. Genomic libraries and a host strain designed for highly efficient two-
515 hybrid selection in yeast. *Genetics*. 144:1425-1436.
516 Kappel, C., U. Zachariae, N. Dolker, and H. Grubmuller. 2010. An unusual hydrophobic core confers extreme
517 flexibility to HEAT repeat proteins. *Biophys J*. 99:1596-1603.
518 Kobe, B., T. Gleichmann, J. Horne, I.G. Jennings, P.D. Scotney, and T. Teh. 1999. Turn up the HEAT. *Structure*.
519 7:R91-97.
520 Kuznetsov, D., F. Tegenfeldt, M. Manni, M. Seppey, M. Berkeley, E.V. Kriventseva, and E.M. Zdobnov. 2023.
521 OrthoDB v11: annotation of orthologs in the widest sampling of organismal diversity. *Nucleic Acids Res*.
522 51:D445-D451.
523 Lang, M.J., J.Y. Martinez-Marquez, D.C. Prosser, L.R. Ganser, D. Buelto, B. Wendland, and M.C. Duncan. 2014.
524 Glucose starvation inhibits autophagy via vacuolar hydrolysis and induces plasma membrane
525 internalization by down-regulating recycling. *J Biol Chem*. 289:16736-16747.
526 Le Bras, S., C. Rondanino, G. Kriegel-Taki, A. Dussert, and R. Le Borgne. 2012. Genetic identification of
527 intracellular trafficking regulators involved in Notch-dependent binary cell fate acquisition following
528 asymmetric cell division. *J Cell Sci*. 125:4886-4901.
529 Liu, K., K. Surendhran, S.F. Nothwehr, and T.R. Graham. 2008. P4-ATPase requirement for AP-1/clathrin function
530 in protein transport from the trans-Golgi network and early endosomes. *Mol Biol Cell*. 19:3526-3535.
531 Longtine, M.S., A. McKenzie, 3rd, D.J. Demarini, N.G. Shah, A. Wach, A. Brachat, P. Philippsen, and J.R. Pringle.
532 1998. Additional modules for versatile and economical PCR-based gene deletion and modification in
533 Saccharomyces cerevisiae. *Yeast*. 14:953-961.
534 Lund, F.W., M.L. Jensen, T. Christensen, G.K. Nielsen, C.W. Heegaard, and D. Wustner. 2014. SpatTrack: an
535 imaging toolbox for analysis of vesicle motility and distribution in living cells. *Traffic*. 15:1406-1429.
536 Martinez-Marquez, J.Y., and M.C. Duncan. 2018. Investigation of Ldb19/Art1 localization and function at the late
537 Golgi. *PLoS One*. 13:e0206944.
538 Mattera, R., B. Ritter, S.S. Sidhu, P.S. McPherson, and J.S. Bonifacino. 2004. Definition of the consensus motif
539 recognized by gamma-adaptin ear domains. *J Biol Chem*. 279:8018-8028.
540 Mirdita, M., K. Schutze, Y. Moriwaki, L. Heo, S. Ovchinnikov, and M. Steinegger. 2022. ColabFold: making
541 protein folding accessible to all. *Nat Methods*. 19:679-682.
542 Noguchi, C., M.V. Garabedian, M. Malik, and E. Noguchi. 2008. A vector system for genomic FLAG epitope-
543 tagging in Schizosaccharomyces pombe. *Biotechnol J*. 3:1280-1285.
544 Pettersen, E.F., T.D. Goddard, C.C. Huang, E.C. Meng, G.S. Couch, T.I. Croll, J.H. Morris, and T.E. Ferrin. 2021.
545 UCSF ChimeraX: Structure visualization for researchers, educators, and developers. *Protein Sci*. 30:70-82.
546 Plemel, R.L., G. Odorizzi, and A.J. Merz. 2021. Genetically encoded multimode reporter of adaptor complex 3
547 traffic in budding yeast. *Traffic*. 22:38-44.
548 Sanger, A., J. Hirst, A.K. Davies, and M.S. Robinson. 2019. Adaptor protein complexes and disease at a glance. *J*
549 *Cell Sci*. 132.
550 Shaner, N.C., R.E. Campbell, P.A. Steinbach, B.N. Giepmans, A.E. Palmer, and R.Y. Tsien. 2004. Improved
551 monomeric red, orange and yellow fluorescent proteins derived from Discosoma sp. red fluorescent protein.
552 *Nat Biotechnol*. 22:1567-1572.
553 Shin, J., A. Nile, and J.W. Oh. 2021. Role of adaptin protein complexes in intracellular trafficking and their impact
554 on diseases. *Bioengineered*. 12:8259-8278.

555 Stockhammer, A., L.S. Benz, S. Harel, V. Natalia, L. Wiench, C. Freund, B. Kuropka, and F. Bottanelli. 2022.
556 When less is more – Endogenous tagging with TurboID as a tool to study the native interactome of adaptor
557 protein complexes. *bioRxiv*:2021.2011.2019.469212.
558 Thomas, P.D., D. Ebert, A. Muruganujan, T. Mushayahama, L.P. Albou, and H. Mi. 2022. PANTHER: Making
559 genome-scale phylogenetics accessible to all. *Protein Sci*. 31:8-22.
560 Tojima, T., Y. Suda, M. Ishii, K. Kurokawa, and A. Nakano. 2019. Spatiotemporal dissection of the trans-Golgi
561 network in budding yeast. *J Cell Sci*. 132.
562 Yoshimura, S.H., and T. Hirano. 2016. HEAT repeats - versatile arrays of amphiphilic helices working in crowded
563 environments? *J Cell Sci*. 129:3963-3970.
564 Yu, Y., A. Kita, M. Udo, Y. Katayama, M. Shintani, K. Park, K. Hagihara, N. Umeda, and R. Sugiura. 2012. Sip1,
565 a conserved AP-1 accessory protein, is important for Golgi/endosome trafficking in fission yeast. *PLoS*
566 *One*. 7:e45324.
567 Zysnarski, C.J., S. Lahiri, F.T. Javed, J.Y. Martinez-Marquez, J.W. Trowbridge, and M.C. Duncan. 2019. Adaptor
568 protein complex-1 (AP-1) is recruited by the HEATR5 protein Laa1 and its co-factor Laa2 in yeast. *J Biol*
569 *Chem*. 294:1410-1419.

570